The visibility of stellar transients in the Galactic Centre

Jonathan Ström

Division of Astrophysics
Department of Physics

LUND
UNIVERSITY

2024–EXA221

Degree project of 15 higher education credits
February 2024

Supervisor: Ross Church

Division of Astrophysics
Department of Physics
Box 118
SE-221 00 Lund
Sweden

Abstract

A semi-analytical simulation was developed to evaluate the K-band magnitudes of Red Giants [0.96 - 1.02 $M_{\odot}$] orbiting the supermassive black hole in the galactic centre. The model assumed star formation between 10-12 Gyrs ago and by following the IMF and applying a random age condition, a stellar population was created. It was established that stars with $m_K \leq 16$ can be observed and then they become too faint and difficult to observe. The magnitude means that Red Giants on and beyond the Red Clump phase are observable, which means only 12% of a total population of Red Giants can be observed.

Secondly mass transfers between the remnants of a Red Giant and a Red Giant star can happen as the dense core passes through the envelope of the star. The result will be a "fuzzball" with observable properties. It showed that larger radius is more important than higher temperature at the region where the envelope is just bound. However after the thermal time scale has passed, the fuzzballs apparent K-band magnitude increases as its luminosity decreases, hence decreasing their observability. This in combination with their cooler temperature and decrease in luminosity would be one way to differentiate them from Red Giants.

It was concluded that if the G2, a stellar gas cloud, orbiting the supermassive black hole is a fuzzball, then it should have a black hole core and be older than 100 000 years since its observed magnitude is higher than expected for the fuzzball model.

Populärvetenskaplig beskrivning

Out there spread all over the night sky are an uncountable amount of stars with a vast range of sizes and properties. They can be redder or they can be bluer, and some are brighter while others can be fainter. The fainter they are, the more difficult they are to observe. The stellar evolution of a star is a long process that can span tens of billions of years. Stars start off in the main sequence phase, where nothing really happens for a few billions of years. The majority of its lifetime is during that stage. When most of its core has been consumed, it becomes more violent, begins to expand and starts changing phase. Turning into a different type of star, and the focus of this paper. Instead of being blueish, it changes colour towards red. Conveniently this phase is named the "Red Giant phase" They continue to grow over their lifetime, becoming brighter as time passes and can be up to a few hundred times larger than our sun. The larger a Red Giant is, the brighter it is. This makes it also easier to observe on the night sky. Interestingly this will eventually happen to our own sun, until it can't grow any larger and collapses in on itself.
What will remain is a dense core. Because there are so many stars in the galactic center, sometimes a Red Giant collides with a core, transferring some of its mass to it, creating a large cover around the core called "fuzzball". When such a collision happen, the fuzzball could be observable because of its enormous size. By finding out how the fuzzball changes with time, it is possible to also see how its visibility changes.

This academic project centers on the topic of "The Visibility of Stellar Transients in the Galactic Center." Our galaxy, the Milky Way circles a Supermassive Black hole in the very center of our galaxy, roughly 8000 parsec away. Although due to the heavy amount of thick dust and gas clouds between us and the center, it is impossible to see with your own eyes. Even with the best telescopes, and imaging in infra red light, it is still difficult to see deep within our galaxy. Unfortunately technology hasn't advanced far enough for us to simply look towards the center and see these violent Red Giants or fuzzballs without difficulties. It is only at a certain stage of their lifetime we are able to observe them. To find out when, I have implemented a computer simulation. By tracking the stellar evolution of the red giants orbiting the Supermassive Black Hole, we get a set range of different stages they can be in. The closer they are to the end of their lifetime, the brighter it appears to be, and the easier it would be to observe them.
This methodical approach is to learn at what stages Red Giants must be in order to be observable in the Galactic Center, and how such a collision between the Red Giant and a dense core would be observable.

Contents

Chapter 1

Introduction

In the Galactic Center (GC), located roughly 8000 parsec (pc) away from Earth, lies the Milky Way's central supermassive black hole, Sagittarius A*. (Abuter et al., 2019) It is surrounded by the Nuclear Stellar Cluster (NSC) which has a radius of 4.2 pc and contains millions of old stars. (Neumayer et al., 2020) (Laurentis et al., 2023) From the works of Schödel et al. (2020) it is known that the NSC had 80% of its star formation circa 10 billion years ago, that then reached a minimum 1-2 billion years later. (Neumayer et al., 2020)

Stellar transients, such as novae, supernovae, and eruptive variable stars happens frequently in our galactic center. (Figer et al., 2004) To observe these phenomena, significant challenges emerge due to the presence of extensive interstellar extinction, which attenuates and scatters mostly optical and ultraviolet light. The interstellar dust grains efficiently extinguish and redden the light (reddening), resulting in a substantial loss of information. This effect is more severe the shorter the wavelength is, making it difficult to detect and characterize the stellar transients. (NASA) (Hannu Karttunen, 2016)

The extinction for the visual range has been measured to $A_V \gtrapprox 38$ for GC observations by Gao et al. (2013), and for near-infrared it was measured to be $A_K = 2.74$ from Nogueras-Lara et al. (2021). Because of this, observations towards the galactic center is mainly done with infrared light (K-band). At the European Southern Observatory, the Very Large Telescope (VLT) is utilized for ground-based observations. NACO, an abbreviation for the combined instrument NAOS+CONICA, has been installed on the VLT. NAOS stands for Nasmyth Adaptive Optics System, an adaptive optics system equipped with both visible and infrared sensors and CONICA servers as the infrared camera and spectrometer which is integrated with NAOS. Together they produce images comparable to those obtained in space. Another facility with telescopes for galactic center observations are the twin telescopes, Keck I- and Keck II adaptive optics systems, located at the Mauna Kea Observatories in Hawaii. It works integrated with a second generation Near Infrared Camera (NIRC-2/AO).

To properly measure the properties of stars and galaxies, photometry and spectroscopy can be used. Photometry takes the approach of directing a telescopes towards a region in space, it measures the incoming electromagnetic radiation through filter bands for a long

exposure period. The sensor, a charge-coupled device (CCD) consisting of pixels representing the area of focus. The pixel will absorb the photons and the number of photons translates to the the number of stored electrons for that area. The more photons that land on a pixel, the brighter the stellar object. From papers Rafelski et al. (2007) and Bartko et al. (2009) it was reported that direct observations towards NSC central region managed to see stars with an apparent magnitude of $m_K \geq 16$

One interesting observation towards the GC is G2, a "cloud-like" stellar body that orbits the SMBH (Gillessen et al., 2012a) (Phifer et al., 2013) (Bower et al., 2015). The origin of the gas-like structure is debatable, where one side states it is nothing more than a gas cloud, while later research have found that it could be the outcome of gas ejected from a compact star (Calderón et al., 2018).
Due to the high density and velocity dispersion of these low mass stars in the NSC, it is expected that collisions happen. From Mastrobuono-Battisti et al. (2021) the collisions between Red Giants and White Dwarfs transfers mass to the envelope of the White Dwarf, making it expand and cool. The transfer of the mass is velocity related meaning that quicker collisions results in a smaller envelope for the WD core (fuzzballs). Depending on the size and luminosity of the envelope, it should be detectable in the K-band similarly to a Red Giant.

1.1 Evolution of stars

The evolution of stars in the proximity of the Galactic Center does not have a constant apparent magnitude throughout their lifetimes. A star deviates from its main sequence by depleting its hydrogen core through nuclear burning, starting the Red Giant Branch (RGB). This causes the core of the star to contract and heat up. A shell of hydrogen around the core begins to undergo fusion, gradually expanding the star, creating a hydrogen rich outer envelope, turning it into a red giant. The luminosity increases, while the temperature decrease, making it more red, hence the name Red Giant.
It continues gradually ascending up the RGB by burning the shell, creating helium in the process. This makes the core heavier, increasing its temperature and speeds up the shell fusion process. The star expands and cools in the envelope, becoming more luminous. At the very edge of the RGB, stars with roughly $1M_{\odot}$ have a helium core supported by electron degeneracy pressure. It is not until the core reaches a high enough temperature that the process of helium fusion starts. Often referred to as the Core Helium Burning Phase (CHeB). During this period of the stars evolution, Helium flashes happens as a large portion of helium is being consumed during a short period inside the core. (Hannu Karttunen, 2016) (Prialnik, 2000) (Thompson, 2014)

The Helium flashes causes the star to become hotter, contract and less luminous as it goes into the horizontal branch, also known as the "Red Clump". This branch is quite eas-

ily identifiable as the Red Giants residing there have a more steady luminosity and colour. (He et al., 2022) As the core slowly contracts, it begins to heat up again over the time span of about 100 millions years. Eventually after burning most of the helium core, the helium shell begins to fuse. The Red Giant gradually expands becoming more luminous. This is the Early Asymptotic Giant Branch (EAGB). (Hannu Karttunen, 2016) (Prialnik, 2000) (Thompson, 2014)

At the end stage of the branch, the helium shell no longer contains any fuel to continue the fusion process. Instead it receives energy from fusion of a thin shell of hydrogen surrounding the helium shell. The process creates additional helium which gradually builds up. It later undergoes violent fusion creating helium shell flashes (pulses) with intense luminosity. It is here the Thermally Pulsing Asymptotic Giant Branch (TPAGB) begins. The helium shell flashes becomes more pronounced and frequent. The core now consists of inactive carbon and oxygen, with a thin layer of burning helium around it. The star continues to expand and increase in luminosity while its temperature deceases. It does so until it no longer undergoes fusion, and the gravitational force overcomes outward pressure from the core. The evolutionary path reaches its climax and gravity contracts the envelope until the outermost layer is emitted and what remains is the hot dense core, also known as a White Dwarf (WD). (Hannu Karttunen, 2016) (Prialnik, 2000) (Thompson, 2014)

By developing semi-analytical models using Python code and utilizing stellar evolution tracks, the first task is to generate a diverse population of Red Giant stars situated in the central region of the Milky Way, more specifically the nuclear stellar cluster (NSC). The observability for the population of stars in the near-infrared will be established.
Secondly the visibility of the extensive envelope surrounding a White Dwarf, referred to as "fuzzballs" following the terminology established in Mastrobuono-Battisti et al. (2021) will also be looked at, to see and compare their visibility to the Red Giant population, and how we could differentiate them.

Chapter 2

Method and Theory

2.1 Stellar Evolution of RGs

2.1.1 MIST: Modeling Stellar Evolution

To simulate the stellar evolution of stars in close proximity to our Supermassive Black Hole (SMBH), Stellar evolution tracks are implemented. The prominent tool in this project is the MESA Isochrones and Stellar Tracks (MIST) project. MIST is based on the Modules for Experiments in Stellar Astrophysics (MESA), an open-source stellar evolution package. MIST takes MESA's stellar evolution tracks and transforms them into isochrones, which presents how stars of varying masses and metallicities evolve from the Main Sequence to critical stages such as the conclusion of hydrogen burning, the cooling phase of a white dwarf, or the conclusion of carbon burning. (Choi et al., 2016).

The stellar evolution tracks provided by MIST follows the four equations for a stars evolution and monitors changes with respect to its radius.

In this project, stars within an initial mass range are considered, following their transition to Red Giants at the conclusion of the Main Sequence phase. The important parameters that will be studied is the luminosity, star age, temperature, and what distinct phases of stellar evolution it takes place in.
By comparing the different MIST files and observing their stellar evolution, I selected those that satisfied the criteria of being Red Giants between 10-12 Gyr of their lifetime, which established a range of 0.96 $M_{\odot}$ - 1.02$M\odot$

Those specific files were implemented into a Python code. The mass range correlates to when most of the stars were formed in the GC from Schödel et al. (2020) and slightly older then the age of formation for the old disk as per research by Xiang and Rix (2022). Figure (2.1) below is an HR-diagram that shows the stellar evolution of a $1M\odot$ star for the luminosity as a function of temperature from a MIST-file.

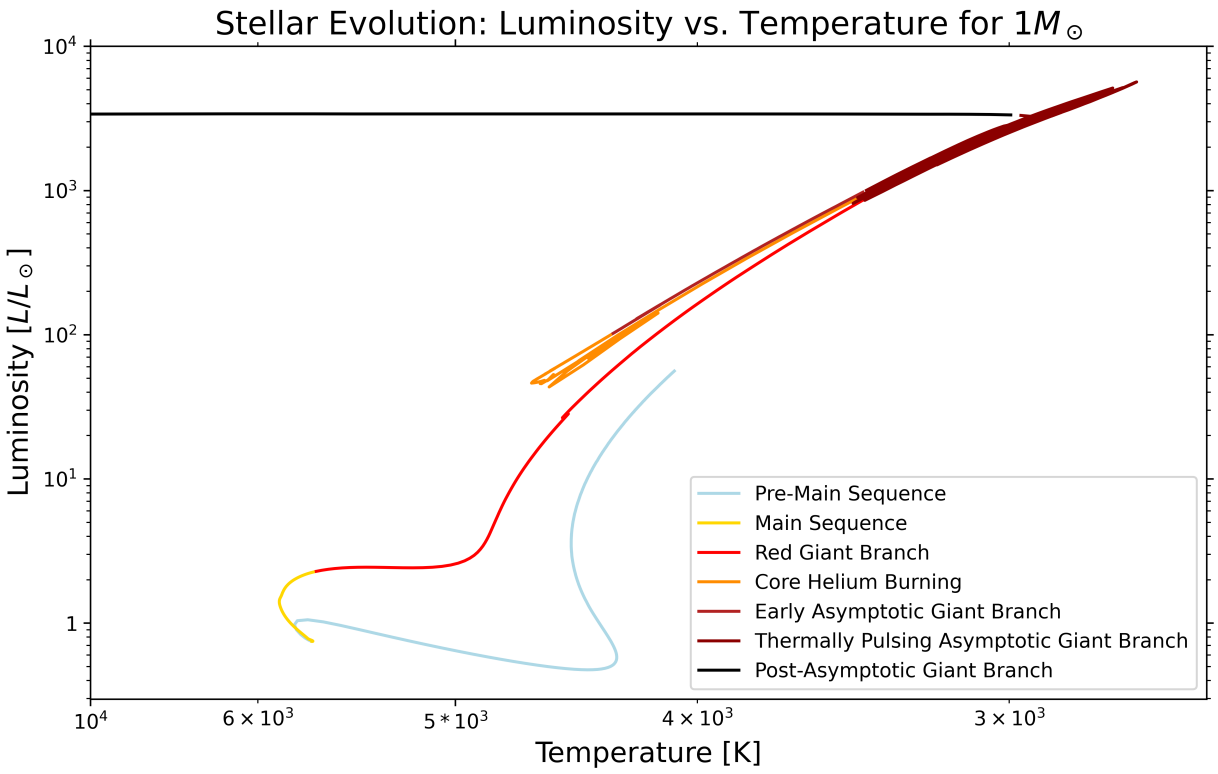

Figure 2.1: A stellar evolution track from MIST of a 1 $M_\odot$ star with solar luminosity vs. temperature

2.1.2 Initial Mass Function

The initial mass function (IMF) refers to the distribution of stellar masses that comes from star formation. It follows the pattern that there is an abundance of massive stars in contrast to lower mass stars. High-mass stars experience an accelerated fusion rate, causing a more rapid depletion of their cores (Wollack, 2010) (Prialnik, 2000). It was first made aware in 1955 by Salpeter when he attempted to measure the luminosity distribution in the Milky Way. The results from this became a power law, named the "Salpeter index" ($\alpha = 2.35$) which is used for masses with the range of $0.4 \lesssim M_\odot \lesssim 10$. This has been supported for some time, however newer studies suggest that an increase for this number should be considered for $M > 1M_\odot$. However for this work, the value was chosen to be $\alpha = 2.35$ (Prialnik, 2000) (Kroupa and Weidner, 2003).

In order to depict the likelihood of star formation relative to the initial mass of stars, a cumulative distribution function (CDF) was used by integrating the IMF

$C(M) = \int_{M_{\min}}^{M} \xi(M')dM'$, where $\xi(M')$ is the probability density function (PDF), $\xi = KM^{-\alpha}$ and K is a constant. Utilizing the CDF for the Initial Mass Function (IMF), the proportion of stars in a population with masses below and above a specified threshold was

determined. Inverting C(M) gives the resulting expression which provides a quantitative representation of the probability associated with stars forming at a given initial mass:

$$M = \left[\left(M_{\max}^{-(1-\alpha)} - M_{\min}^{-(1-\alpha)}\right) C(M) + M_{\min}^{-(1-\alpha)}\right]^{\frac{1}{-(1-\alpha)}} \tag{2.1}$$

Where M_{max} is the initial mass of a star at which was chosen to be $1.02M_{\odot}$, M_{min} is the initial mass of a star and was chosen to be $0.96M_{\odot}$ and α is the Salpeter index influencing the shape of the IMF distribution (Prialnik, 2000).

Utilizing the CDF in the python code were C(M) was a random variable [0,1], a simulation was developed for 1000 stars using the MIST files. The files were loaded and selected through the density probability of the IMF. With 1000 stars following the curve, a random star age condition was implemented. Each star received a random age falling between the 10-12 Gyr condition. The random age also provided the corresponding stellar phase, temperature (T) and luminosity (L) through the MIST-file. This approach was adopted to account for the expected diversity in ages for the Red Giants orbiting the Supermassive Black Hole.

2.1.3 Linear Interpolation

Linear interpolation involves approximating values between two known data points by drawing a straight line on a graph. The unknown point's value is then determined based on its position along this line, which provides an efficient way to estimate a value within a specific range as is given by:

$$y = y_1 + \frac{(y_2 - y_1)}{(x_2 - x_1)}(x - x_1)$$

where the known values are plugged into each variable. (Kong et al., 2021)

2.1.4 Photometry, Bolometric Corrections & Magnitudes

In the paper Lejeune et al. (1998) a table has been created for observable parameters of Red Giants with different metallicities. However the table does not take into account Red Giants with temperature below 2500 K, as they are extremely rare in nature and short lived on the cosmological timescale. To solve the issue of low temperature Red Giants, a combined effort of Lejeune et al. (1998) and a linear interpolation was created. It contains the temperature, colour bands V-K and H-K, and the bolometric correction in the V-band for Red Giants with a variety of temperatures for metallicity [M/H = 0]. The choice of having 0 metallicity stems from assumptions that there are a large range of stars in the center with different properties and history, making it difficult to approximate a "correct" value. However in this project, the simulation of stars have roughly the same properties as our sun and can therefore be assumed to also share its metallicity.

Table 2.1: Combined Data for values of the (V-K) colour bands, (H-K) colour bands and the bolometric correction in the visual band (BC_V) for Red Giants with Metallicity [M/H = 0]

$T_{\text{eff}}[K]$	$V-K$ [mag]	$H-K$ [mag]	BC_V [mag]
100	14.152	0.658	-10.166
250	13.866	0.645	-9.921
500	13.388	0.623	-9.513
750	12.911	0.602	-9.104
1000	12.433	0.580	-8.696
1250	11.956	0.558	-8.288
1500	11.478	0.537	-7.879
1750	11.001	0.515	-7.471
2000	10.523	0.493	-7.063
2250	10.046	0.472	-6.654
2500	9.568	0.450	-6.246
2800	8.995	0.424	-5.756
3000	8.458	0.391	-5.343
3200	7.232	0.359	-4.241
3350	6.292	0.314	-3.368
3500	5.487	0.258	-2.688
3750	4.228	0.212	-1.586
4000	3.475	0.157	-1.037
4250	2.992	0.140	-0.731
4500	2.613	0.107	-0.544
4750	2.234	0.074	-0.357

Photometry is the process of measuring the brightness of celestial bodies and objects through filters (Bands) that observes with different wavelengths. The colour index, denoted as $V-K$, is a quantitative measure of the difference between the magnitude - a measure of the difference in how bright a star is - through two distinct bands. V represents the visual magnitude band of wavelengths around 550 nm. This roughly translates to green-yellow light. The K-band magnitude (K), which is common for deep stellar observations, represents the magnitude in the near-infrared at circa 2.2 μm. As interstellar dust and gas reddening light as small wavelengths are absorbed, the difference between the magnitudes is used to correct the reddening effect. (Allen, 1973)

Likewise, the color index $H-K$ represents the magnitude difference of the H-band, which has a wavelength of approximately 1.6 μm. Similar to the K-band, the H-band also falls within the near-infrared spectrum (Allen, 1973).

BC_V is called the bolometric correction in the Visual band (V-band). It is a correction factor since a star will emit radiation across a broad spectrum, while the V-band only

takes into account a specific portion of the spectrum. (Hannu Karttunen, 2016) (Eker et al., 2021)
By taking the temperature of the selected mass star following the CDF, the temperature can then be linearly interpolated through the values of table (2.1). By proceeding a corresponding bolometric correction value for the visual band was received. The very same process happens for the colour indices (V-K) and (H-K). BC_V can be made into the bolometric correction for the K-band (BC_K) by the following equation from Hannu Karttunen (2016) and Allen (1973):

$$BC_K = BC_V - (V - K) \tag{2.2}$$

where BC_V and $(V - K)$ was received through linear interpolation with the corresponding temperature. (Hannu Karttunen, 2016) The next step is to calculate the absolute bolometric magnitude, which measures the total intrinsic luminosity of a celestial object across all wavelengths:

$$M_{\text{bol}} = M_{\text{bol}_\odot} - 2.5 \log_{10} \left(\frac{\text{L}}{L_\odot} \right) \tag{2.3}$$

where $M_{\text{bol}_\odot} = 4.74$ is the absolute bolometric magnitude of the Sun. (Hannu Karttunen, 2016).

From Eker et al. (2021) the absolute magnitude of a star can be calculated by equation (2.3) and equation (2.2). The absolute magnitude of a star quantifies its intrinsic brightness, showing what the apparent magnitude the star would exhibit at a distance of 10 parsecs (equivalent to 32.6 light-years) away from the observer. (Eker et al., 2021):

$$M_K = M_{\text{bol}} - BC_K \tag{2.4}$$

Additionally the absolute magnitude in the H-band is also easily determined and can be solved for by this.

$$M_H = M_K + (H - K) \tag{2.5}$$

Insintric means that it has been corrected for the extinction, so the light has not been absorption and scattering dust along the line of sight. With the equation (2.4) and equation (2.5) the intrinsic colour index of the H-K band was acquired:

$$(H - K)_0 = M_H - M_K \tag{2.6}$$

With the received value of M_K the next step is to find the apparent magnitude (m_K). It is defined as the actually measured magnitude, or how bright the star appears to be, from Earth and through extinction. Following Hannu Karttunen (2016) it is written as:

$$m_K = M_K + A_K + 5 \log_{10} \left(\frac{d}{10} \right) \tag{2.7}$$

However the extinction throughout the galaxy is not a constant. Different parts of the galaxy have different extinctions values because of the layers of dust and stellar clouds. A paper by Nogueras-Lara et al. (2021) found by photometry from the GNS survey, that the average extinction coefficient in the K-band for the galactic centre $A_k = 2.74$. However the paper only considered light coming from active stars, and not from other celestial bodies. By creating a Gaussian fit over their extinction map, a slightly different average result from the peak was concluded. With a new value for A_K which is chosen to be constant, equation (2.7) was solved and together with equation (2.6) a color-magnitude diagram was plotted by repeating the process 1000 times, for the 1000 stars simulated in the GC.
The simulation afterwards was initiated again, however the second time a population of stars and their m_k value was plotted.

2.1.5 Fuzzball model

In Mastrobuono-Battisti et al. (2021) they go over the predictions of something that they refer to as "fuzzballs". It is expected that Red Giants experience occasional encounters with stellar objects that are much denser than their envelopes. Such objects could be main sequence stars, White Dwarfs (WD) or black holes. The collisions does not annihilate the compact objects, or the Red Giant, but instead a mass transfer happens in which the Red Giant loses a portion of its mass. This creates a low-mass envelope for the compact object which has a luminosity. The dense core with a luminous envelope is referred to as a fuzzball.

Fuzzball Structure

The assumption is that the weak envelope reaches hydro-static equilibrium and then follows the equations of stellar evolution. By solving the stellar equations a relationship for the observable characteristics of the fuzzball, a relationship with its Radius (R), effective temperature (T) and luminosity (L) can be made with the stellar cores mass (M_{core}), the mass of the envelope (M_{env}) and the thermal time scale of the fuzzball envelope ($\tau_{th,env}$). The thermal time scale is the period of how long the envelope exist before it begins to shrink. Since the fuzzball does not produce energy in its core from fusion, it will decrease in radius as energy is radiating away at the surface.

The assumption is made that the envelope of the object is prone to convective activity, leading to the rising and falling of material within the envelope, creating currents and mixing. Under this assumption, the conditions within the envelope are such that entropy remains constant during these convective motions. The specific ratio of specific heats, denoted as $\gamma = \frac{5}{3}$, is applied because the atoms in the envelope have three degrees of freedom. This particular ratio is common for monotonic gases and is frequently utilized in astrophysics. From there the pressure (P) is written as:

$$P = K\rho^{\frac{5}{3}} \tag{2.8}$$

where $\mathcal{R}$ is the gas constant with a value of $\mathcal{R} = 8.314\ kg^{-1}K^{-1}$, $\mu = 0.7$ is the mean molecular mass and K is a constant determined by the ideal gas equation of state at the surface with surface density (ρ_s).

$$K = \frac{\mathcal{R}T}{\mu\rho_s^{\frac{2}{3}}} \tag{2.9}$$

Mastrobuono-Battisti et al. (2021) continues by finding the density of the envelope $\rho(r)$ by deriving equation (2.8) with respect to radius (r). The function is then integrated with respect to the radius and the density is solved for. The end result becomes:

$$\rho(r) = \{\rho_s^{\frac{2}{3}} + \frac{2GM_c}{5KR}(\frac{R}{r} - 1)\}^{\frac{3}{2}} \tag{2.10}$$

where $\rho_s^{\frac{2}{3}}$ is the surface density, $G = 6.67430 \cdot 10^{-11}$ is the gravitational constant, $M_c = 0.55 M_\odot$ and r is the radial co-ordiante, that describes the distance from the center to the fuzzy envelope.

With a envelope density acquired it is simple to also acquire the mass of the envelope:

$$M_{env} = \int_{R_c}^{R} 4\pi r^2 \rho(r) dr \tag{2.11}$$

where $R_c = 0.1 R_\odot$ is the base radius of the envelope and R is the radius of the fuzzball. To be able to receive the envelope mass, first the surface density must be found so equation (2.10) can be solved for. In the paper Mastrobuono-Battisti et al. (2021) a grey surface boundary condition is implemented for the gas pressure at the surface of the envelope and its opacity. It means that the radiation field remains a black body all the way out to the surface. By rearranging the equation a function for the opacity and surface density is obtained.

$$\rho_s \kappa(\rho_s, T) = \frac{2GM_c}{3R^2} \cdot \frac{\mu}{\mathcal{R}T} \tag{2.12}$$

R and T are the only parameters that can be chosen, while the remaining are constants. To finally extract the surface density (ρ_s), a bicubic spline fit to the opacities taken from Ferguson et al. (2005) is performed. The opacity is based on the parameter ρ_s and T. The script begins by creating a 2D grid with T vs B. Here B is defined as $B = \frac{\rho}{T_6^3}$ where the temperature is in million degrees. This can be rearranged so that $T_6^3 = (\frac{T}{10^6})^3$. The opacity data is then extracted and utilized to construct the bicubic spline interpolator by subtracting the right hand side, making the function equal to 0. The process initialises by defining initial density values for the set row of T and iteratively refining these values using a bisection method until convergence is achieved.
With ρ_s found, the density of the envelope can be determined with eq: (2.10) and with $\rho(r)$ the envelope mass can also easily be determined

Following the work in Mastrobuono-Battisti et al. (2021) the internal energy of the envelope is solved for by using the ideal gas law for a monotonic gas:

$$U = \int_{env} \frac{3}{2} \frac{\mathcal{R}T}{\mu} dm = 6\pi K \int_{R_c}^{R} r^2 \rho(r)^{(\frac{5}{3})} dr \tag{2.13}$$

And the gravitational potential energy is described by:

$$\phi = -\int_{env} \frac{GM_c}{r} dm = -4\pi G M_c \int_{R_c}^{R} r\rho(r) dr \tag{2.14}$$

If the total energy was positive, i.e larger than zero, the envelope would not be bound to the dense core. The thermal time scale as mentioned previously is how long the envelope lasts before radiating away all of it its internal energy at its current surface luminosity. It is an approximation and can be described as:

$$\tau_{th,env} = \left| \frac{\Phi + U}{L} \right| \tag{2.15}$$

Where L is the luminosity of the envelope mass given by $L = 4\pi R^2 \sigma_{sb} T^4$ and $\sigma_{sb} = 5.67 \cdot 10^{-8} W \cdot m^{-2} \cdot K^{-4}$ is the Stefan-Boltzmann constant. It is important to note that the luminosity is only appearing from the envelope, so the thermal time scale does not take into account the luminosity of the compact core within the fuzzball.

Evolution of Fuzzball

With the envelope mass acquired it is expected that it remains constant with respect to change in time. Since the dense core does not evolve anymore and it has already accumulated the mass from a Red Giant. The total differential of the mass of the envelope with constant T and radius (R) is then described by

$$\frac{dM}{dt} = \frac{\partial M}{\partial R}\bigg|_T \cdot \frac{dR}{dt} + \frac{\partial M}{\partial T}\bigg|_R \cdot \frac{dT}{dt} = 0 \tag{2.16}$$

The change in energy decreases over time as the energy radiates away. The total differential of the envelope energy with constant T and radius (R) can similarly be written as:

$$\frac{dE}{dt} = \frac{\partial E}{\partial R}\bigg|_T \cdot \frac{dR}{dt} + \frac{\partial E}{\partial T}\bigg|_R \cdot \frac{dT}{dt} = -L \tag{2.17}$$

Where for convenience $\frac{dR}{dt}$ and $\frac{dT}{dt}$ is written as $\dot{R}$ and $\dot{T}$, respectively.
The application of the total differential to the fuzzball model aims to derive an expression describing temperature and radius as a function of time. Similar to stars, the magnitude in which we could observe fuzzballs corresponds to their temperature and radius, which additionally is linked to luminosity, as can be seen above. By monitoring the evolution of these parameters, the objective is to observe how the fuzzballs apparent magnitude undergoes changes over time.

To continue the process, $\dot{R}$ can be singled out from equation (2.16)

$$\dot{R} = -\dot{T} \cdot \frac{\frac{\partial M}{\partial T}\big|_R}{\frac{\partial M}{\partial R}\big|_T} \tag{2.18}$$

Then plugging equation (2.18) into equation (2.17), it can be solved for $\dot{T}$

$$\dot{T} = \frac{-L \cdot \frac{\partial M}{\partial T}\big|_R}{\frac{\partial M}{\partial R}\big|_T \cdot \frac{\partial E}{\partial T}\big|_R - \frac{\partial E}{\partial R}\big|_T \cdot \frac{\partial M}{\partial T}\big|_R} \tag{2.19}$$

With a function for $\dot{T}$, it can be plugged into equation (2.18), expanding it and giving the complete function:

$$\dot{R} = \frac{L \cdot \frac{\partial M}{\partial T}\Big|_R}{\frac{\partial M}{\partial R}\Big|_T \cdot \frac{\partial E}{\partial T}\Big|_R - \frac{\partial E}{\partial R}\Big|_T \cdot \frac{\partial M}{\partial T}\Big|_R} \tag{2.20}$$

Here the partial derivatives follow the classical definition of partial derivatives with respect to the initial conditions. They need to be determined numerically and are expressed as follows:

$$\frac{\partial M}{\partial R}\Big|_T = \lim_{\delta R \to 0} \frac{M(R+\delta R, T) - M(R,T)}{\delta R}$$

$$\frac{\partial M}{\partial T}\Big|_R = \lim_{\delta T \to 0} \frac{M(R, T+\delta T) - M(R,T)}{\delta T}$$

$$\frac{\partial E}{\partial R}\Big|_T = \lim_{\delta R \to 0} \frac{M(R+\delta R, T) - M(R,T)}{\delta R}$$

$$\frac{\partial E}{\partial T}\Big|_R = \lim_{\delta T \to 0} \frac{M(R, T+\delta T) - M(R,T)}{\delta T}$$

To determine the numerical values of these partial derivatives, each function was plotted against its corresponding δC coefficient, where C is either T or R. A sufficient flat linear value was chosen from the plots to represent each partial derivatives convergence. With it, equation (2.19) and equation (2.20) could be solved. The figures for each of the partial derivatives can be seen in figure (2.2) below. The convergence of each partial derivative is a result of the δC function approaching zero, in spite of that it can be seen in (4.4a) and (4.4b) that as δR and δT approaches zero for really small values, the partial derivative becomes uncertain. This is the result of numerical error evaluated as $\delta C \to 0$, that arises due to the numerical precision of such small values. The values chosen from 2.2 is a compromise between inaccuracy and convergence. For high values of δC, it diverges, and for significantly small values, the function diverges once again due to numerical imprecision. From figure (2.2) each partial derivative numerical value was established from observing the convergence, and was then expressed in $\dot{T}$ and $\dot{R}$ from equation (2.19) and equation (2.20).

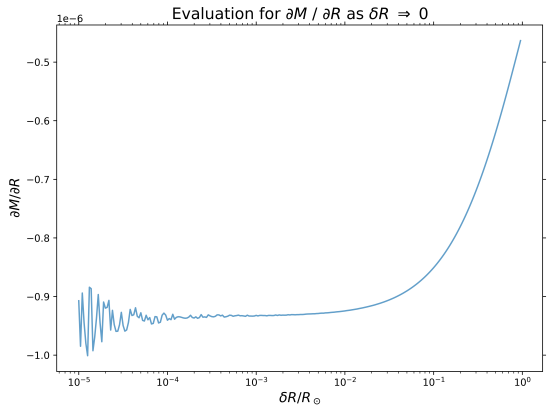

(a) Numerical value for $\delta R = 2 \cdot 10^{-3}$ was chosen as $\delta R \to 0$

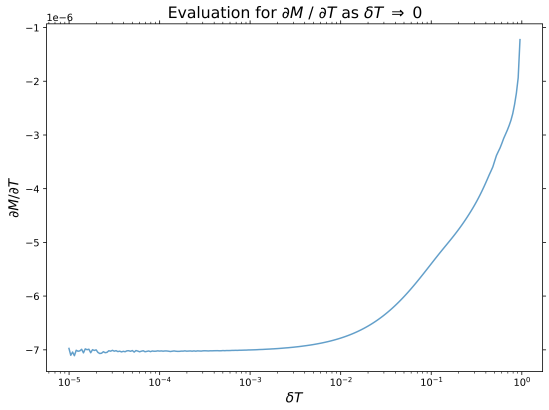

(b) Numerical value for $\delta T = 2 \cdot 10^{-4}$ was chosen as $\delta T \to 0$

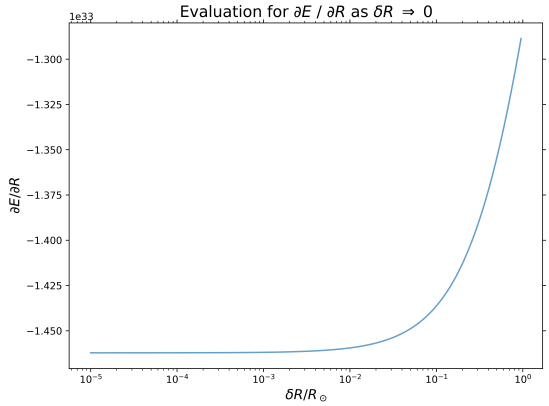

(c) Numerical value for $\delta R = 2 \cdot 10^{-4}$ was chosen as $\delta R \to 0$

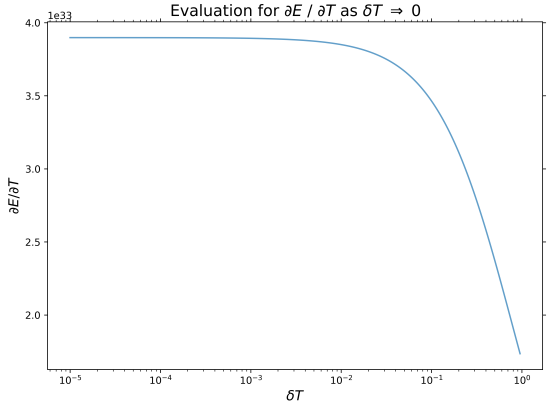

(d) Numerical value for $\delta T = 2 \cdot 10^{-4}$ was chosen as $\delta T \to 0$

Figure 2.2: This figure displays the convergence of each partial derivative and the chosen flat region where it does not diverge due to numerical imprecision for low values, as can be seen in the top two figures.

Reported in Mastrobuono-Battisti et al. (2021), it was demonstrated that a boundary exists in the log T - log R plane between the bound- and unbound state for a fuzzball. The assumption is that at the fuzzballs are born on the boundary with the maximal radius of the envelope and a heightened luminosity resulting from lower temperatures. This circumstance hints a collision event, leading to a large mass transfer to the WD core. $\dot{T}$ and $\dot{R}$ are taken as boundary conditions for the fuzzball and are then solved for using the Runge–Kutta method, which is a numerical approach utilized for approximating solutions to ordinary differential equations. It involves iterative steps to update the solution at discrete points, combining information from multiple stages within each step. (Zheng and Zhang, 2017) The outcome from the method was the expression for temperature at time $T(t)$ and the radius at time $R(t)$

To begin with $T(t)$ was evaluated near the boundary at $t = 0$. The temperature changes as time passed was linear interpolated with data from Table (2.1) to get out BC_K from equation (2.2), M_{bol} from equation (2.3) and M_K from equation (2.4). The apparent K-band magnitude could finally be solved for using equation (2.7). The process was repeated for different boundary conditions from the mass transfer. Table (2.2) below shows the boundary conditions taken from the bound / unbound state of Mastrobuono-Battisti et al. (2021) work. The values at the boundary corresponds to a WD core of 0.55 $M_\odot$

Table 2.2: boundary temperature and radius data at the boundary of a fuzzball with a $0.55 M\odot$ WD core

Temperature [T] (K)	Radius [R/$R_\odot$]
1291	6968
775	11600
465	19300
280	32000
167	54000
100	90000

The apparent K-band magnitude and how it changes was plotted over time. Additionally the temperature and radius of the envelope over time was also calculated using Runge-Kutta solution for equation (2.19) and equation (2.20) respectively. This allowed to observe how the boundary conditions changes with m_K as temperature and luminosity radiates away.

Chapter 3

Result

3.1 Stellar Evolution of Red Giants

Figure (3.1) below was acquired from the paper Nogueras-Lara et al. (2021) where they created a extinction map for the NSC based on $H - K$ colours. It was done by using photometry in the system NACO on the VLT for 7738 stars. By taking the number of light-sources (pixels) on the extinction map against A_K, the range was plotted with a Gaussian distributions fitted over the range.

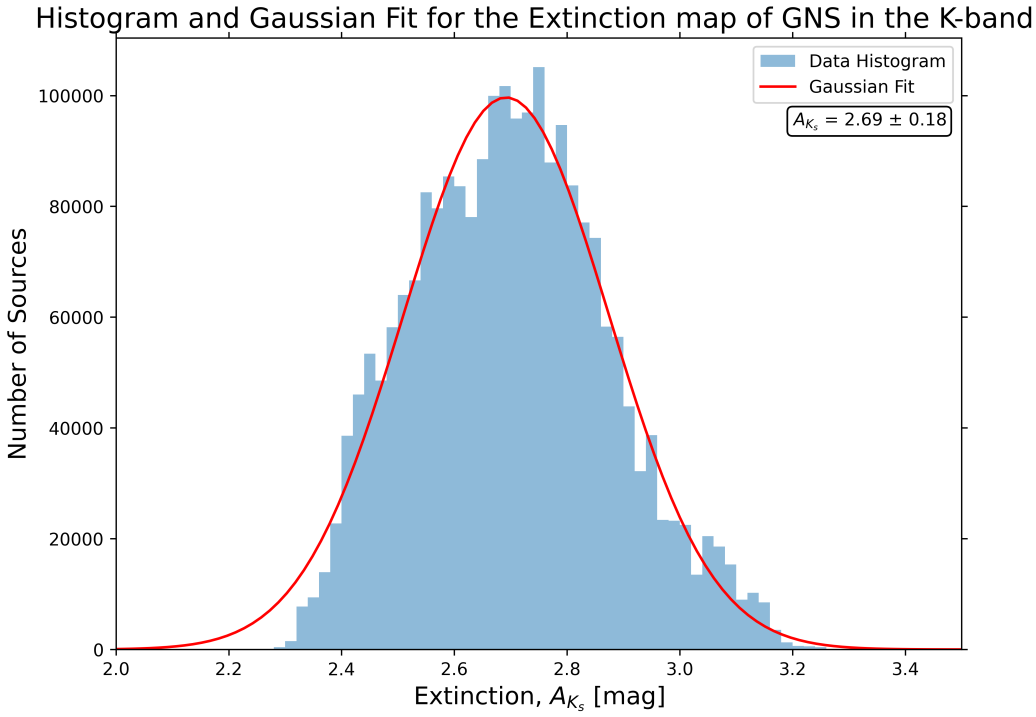

Figure 3.1: The extinction coefficient $A_K = 2.69 \pm 0.18$ for observations directed towards the galactic center.

Attempting to get the same result as in Nogueras-Lara et al. (2021) yielded a different result of $A_K = 2.69$, as seen in figure (3.1), compared to the one from the paper $A_K = 2.74$. However the distribution is slightly skewed and outside the Gaussian for some regions. In Nogueras-Lara et al. (2021) paper, instead of taking the Gaussian distribution of the A_K values, they took the median. It is important to note that obviously the extinction does not remain constant throughout the universe, or in this, case towards the galactic center. It changes depending on where the stellar objects are in the NSC (Bosma, 2023). To put the extinction variable as a constant would not be a fair representation. However in most of the applications in this paper, it will be used as a constant $A_K = 2.69$. I chose although to continue with the Gaussian since I will use the distribution later to do a sweep of A_K values for a population of stars.

Figure (3.2) below was the achieved result with the MIST-files with the initial mass range of 0.96-1.02 $M_\odot$ by plotting the apparent magnitude m_K vs. time. It was performed by linear interpolation of table (2.1) and inserting the values into equation (2.2), equation (2.3), equation (2.4) and finally to be concluded in equation (2.7). Here the constant extinction value of $A_K = 2.69$ was used.

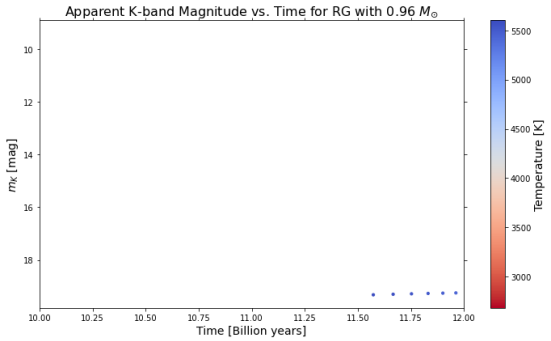

(a) Stellar evolution for a 0.96 $M_\odot$ Red Giant

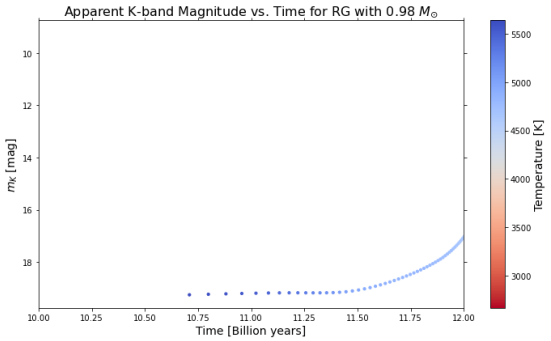

(b) Stellar evolution for a 0.98 $M_\odot$ Red Giant

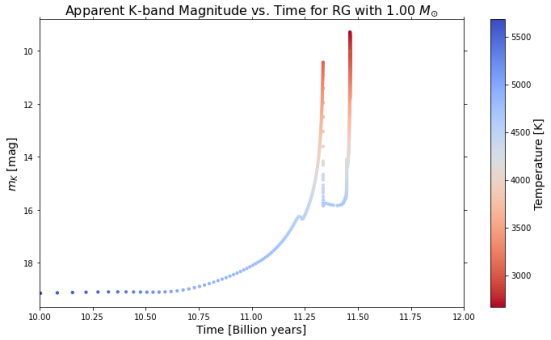

(c) Stellar evolution for a 1.00 $M_\odot$ Red Giant

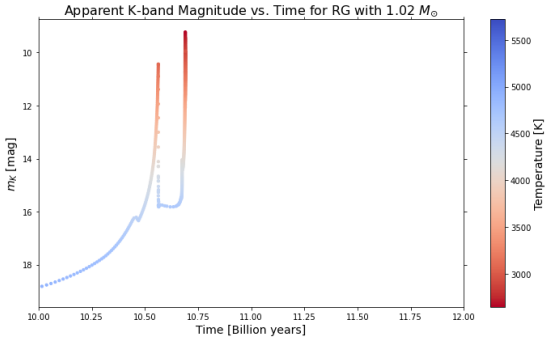

(d) Stellar evolution for a 1.02 $M_\odot$ Red Giant

Figure 3.2: The plots show the stellar evolution for RG-stars as apparent magnitude m_K as time. Additionally it displays the criteria for each star having its Red Giant phase within the 10-12 Gyrs initial condition

In the top left figure, the $0.96M\odot$ stars begins their RG-phase at roughly 11.55 Gyrs. Only the beginning phase of the RG was considered as the later evolution falls beyond the initial time condition. Because of the later evolution into the Red Giant branch, the stars with this initial mass have a high magnitude of $m_K \approx 19$ and will be much more difficult to observe, compared to later Red Giant phases.

The top right figure with $0.98M\odot$ stars begins their red giant phase past the beginning of time constraints, at $t = 10.8$ Gyr. Therefore not much of the stellar evolution takes places within the time-limit as the RGB is a long process. The temperature only drops a small fraction as it continues to evolve and reaches a value of $m_K \approx 17$ before the time condition is reached. Which is just before the "knee" or bump on the plot. This bump is where the Red Clump (RC)/ Horizontal branch resides. This lower magnitude makes it slightly more observable compared to $0.96M\odot$ stars.

At the bottom left figure, the stars with $1M\odot$ have just become Red Giants by 10 Gyrs. Its entire stellar evolution takes place within the time limit. The RC at 11.2 Gyrs is the period in which core helium burning begins. At 11.3 Gyrs it has descended down

the EAGB branch and depleted the helium- core and shell. The increase in m_K at 11.4 is from the start of the TPAGB until the core collapses. From this timescale it is clear that Red Giant stars are the most observable during EAGB phase and TPAGB phase, where temperature decreases drastically. However the issue lies in the incredibly short time scale during those branches.

Bottom right highlights that more massive stars finish their nuclear burning much faster than their lower-mass counterpart. $1.02M_{\odot}$ stars have most of their long Red Giant Branch before the time condition, resulting in the later phases taking place much earlier on the cosmic time scale.
All the four figures follow the same stellar evolution path, just at different times. The range of apparent magnitudes are unchanged, as well as the temperatures.

The MIST files was selected through the Cumulative Distribution Function (2.1) and repeated 1000 times to simulate 1000 stars. To not have stars of the same age, a random age condition was implemented that came into effect when a MIST file was selected. The star received a random age between 10-12 Gyrs which could only be given if the star has a phase during that period. If no phase was found, a new random age was selected.

By solving equation (2.6) and equation (2.7) a Instrinsic Colour-Magnitude Diagram (CMD) was plotted and can be seen below in figure (3.3).

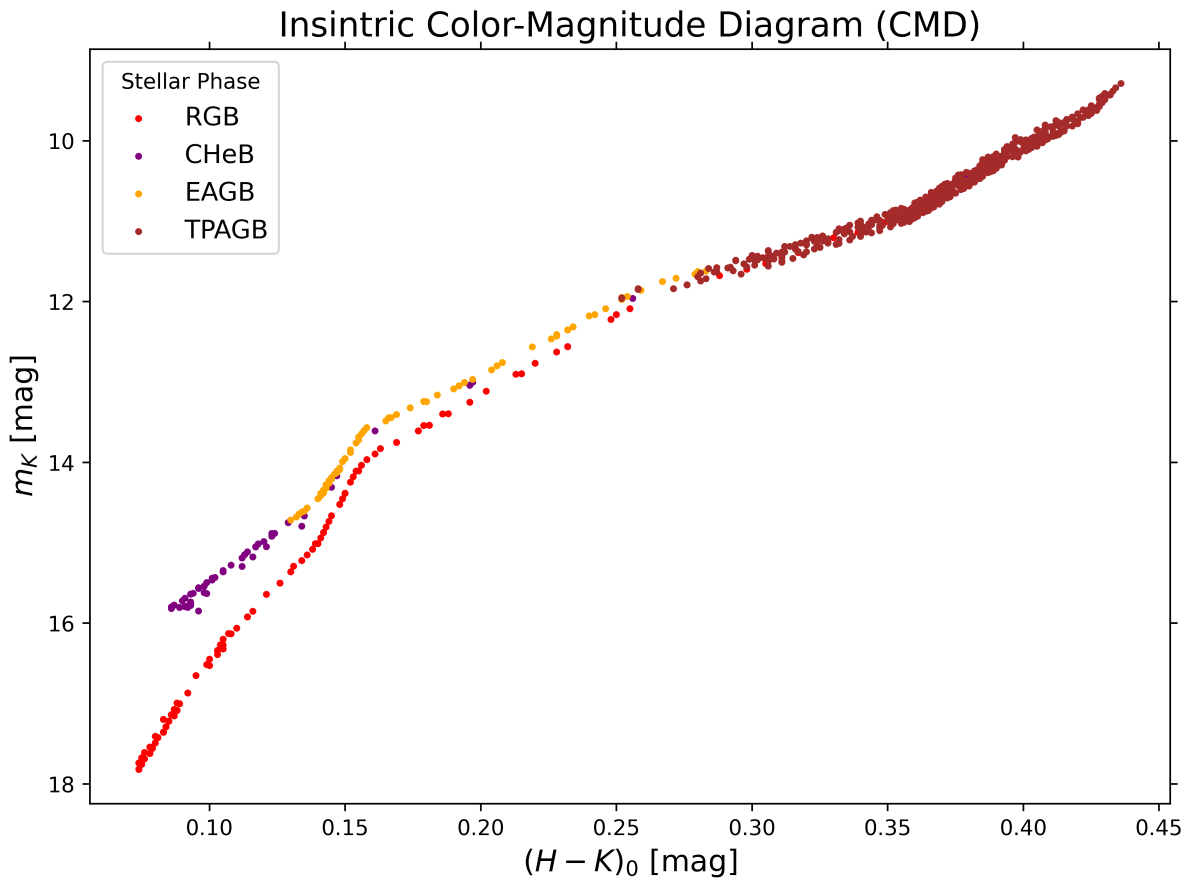

Figure 3.3: This shows the apparent magnitude m_K vs. the intrinsic colour index $(H-K)_0$ for 1000 stars in a variety of phases and ages, with the constant extinction value $A_K = 2.69$

In figure (3.3) above the relationship between the apparent magnitude and the intrinsic colour band $(H-K)_0$ is visualised. It is made clear that the later phase TPAGB have the lowest m_K value with a minimum of around 10 magnitudes and hence is easier to observe than stars in the Red Giant Branch (RGB). This falls in line with the heightened luminosity from the radius of the RG at that stage. It is however cooler, which effects the luminosity function negatively, but since the range of temperature is between 2500-5500 K from figure (3.2) and scales squared, compared to radius which scales to the power of four, so the K-band magnitude will evidently be lower. The intrinsic colour magnitude additionally tells us that those stars are much redder, which is what to be expected as the radius is enormous due to expansion and cooler temperature. The two lines can be explained by referring to figure (2.1). Different phases of the Red Giant can have the same luminosity, hence the same m_K values but not $(H-K)_0$ values. The result is two lines where the stages CHeB and EAGD have a lower m_K magnitude for the same intrinsic colour as a RGB star. Naturally overlapping for the phases are present for the different phases as the temperature is sometimes cooler for a RGB star than they are for a TPAGB star figure (2.1).

Here 60000 stars are plotted as a function of their m_K value. The Gaussian distribution of A_K values was used instead of a constant value. The work was made as an attempt to simulate the observations from Schödel, R. et al. (2010), which shows the observed K-band magnitude of 7738 stars in the GC. To compare, the observational data has been over-plotted on my figure. The same process was used as before by taking the stars based on the CMD with the random age condition, but instead taking the number of stars that would have approximately the same K-band apparent magnitude.

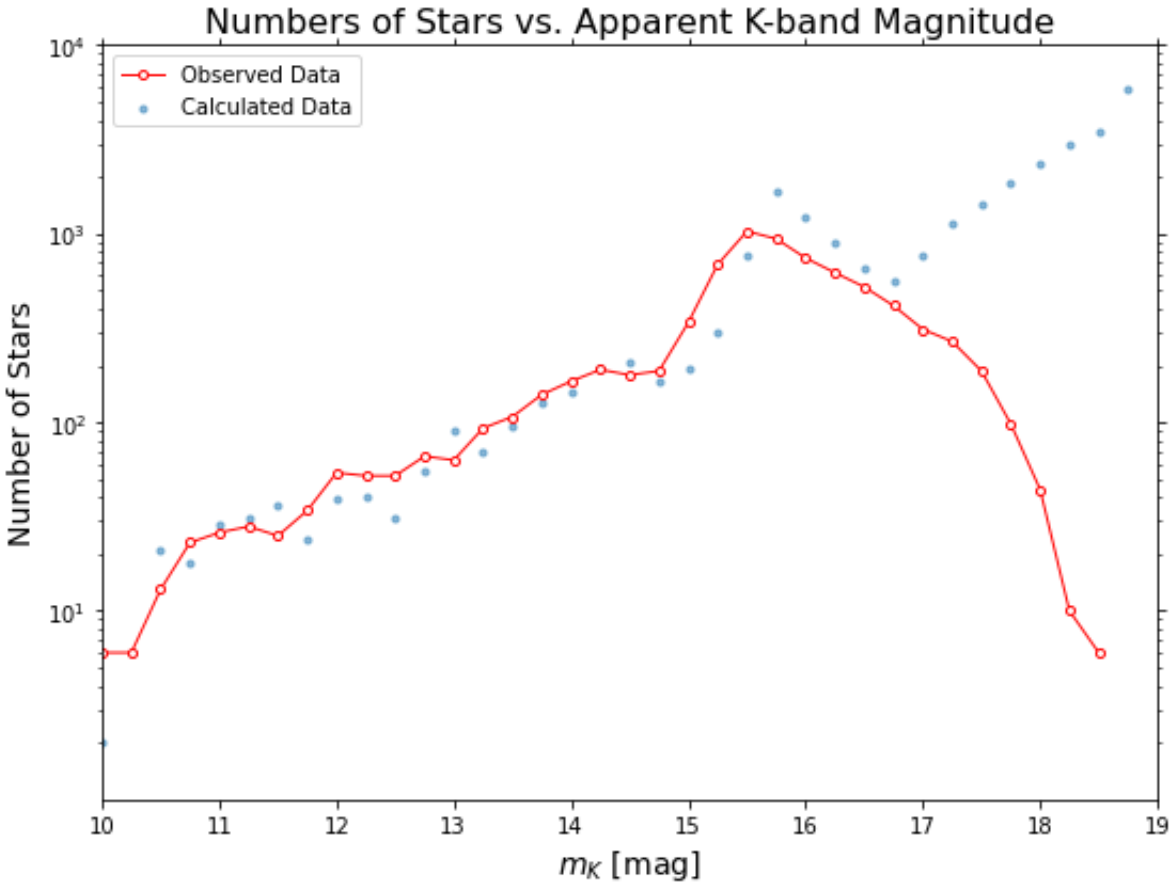

Figure 3.4: The number density of stars vs. the apparent magnitude m_K for approximately 60000 stars orbiting the SMBH following a distribution of A_K values. The observed data for 7738 stars have been plotted over

My simulation of 60000 stars follows the observations very well. Of course there is some deviation as my figure have some randomness too it following the random age condition. It is also different after the RC at $m_K = 16$, where our observations naturally drop off due to the stars being to faint to observe, while my theoretical data keeps going. The population of Red Giant stars that we are able to observe is approximately 12% of the total population. From this we can see how uncommon those bright and late-phase stars

are, and shows that there are a lot more RG stars with fainter magnitudes which are much more difficult to observe.

The sweep is a nicer way to approximate the extinction towards the galactic center due to its variability. Each star received a value of A_K corresponding to its probability from its Gaussian and with equation (2.7) it was solved the same way as previously. The fraction of low m_K stars compared to high falls within expectation because on the cosmological timescale, a star spends a very short time on the later evolutionary phases, where it is the brightest. The small bump around $m_K = 15.75$ is the Red Clump / Horizontal branch and contains more stars because of its stability in temperature and its phase-period, which can be seen in figure (3.2) and follows the observations quite well.
It is noteworthy to know that the difference in a constant A_K value and doing a sweep is minuscule. The difference in the extinction from the maximum value to the minimum value is essentially one magnitude, and in figure (3.4) the stars were assigned to its nearest .25 value since the stars were selected at a random age, which would corresponding to a very specific m_K value and no two stars would have the exact same value. Even with a constant A_K value the figure would look roughly the same.

From the works of Rafelski et al. (2007) and Bartko et al. (2009) the observed apparent K-band magnitude is approximately $m_K \leq 16$ for differentiating Red Giants from early type stars, which means that the observable region for photometry and spectroscopy for Red Giants, can be drawn at the Red Clump and below. The population of those stars are only one tenth of the total population as predicted by the figure. Observations can still be made, however with more difficulty and the dropout for the observations seems to go towards 19-20 m_K.

3.2 Fuzzballs

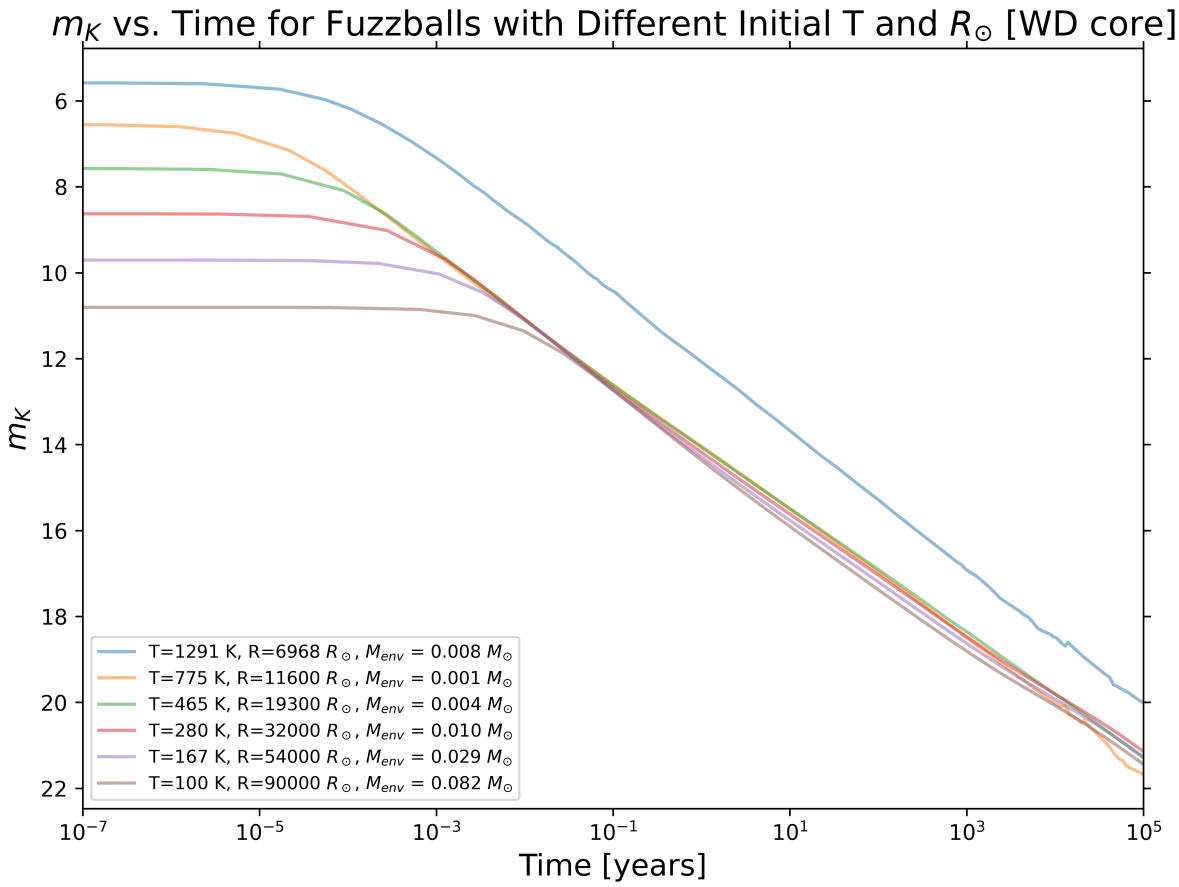

Figure 3.5: The apparent magnitudes m_K for fuzzballs with WD core (0.55 $M_\odot$) vs. time.

In figure (3.5) fuzzballs apparent K-band magnitude has been plotted against time for different initial boundary conditions using equation (2.7). This is the point where the fuzzball is on the verge of being unbound due to its size and temperature. It was achieved by taking the interpolated values of the boundary conditions following table (2.1). It is noticeably that the fuzzballs at the boundary from Mastrobuono-Battisti et al. (2021) are the most visible for the first eight hours ($\sim 10^{-3}$ years). This is of course is the limit for the thermal time scale as given by equation (2.15) which tells how long it takes for a star to emit all of its kinetic energy at the rate of its luminosity. Which is precisely why lower temperature fuzzballs begin to decrease their brightness later.

A interesting aspect of the fuzzball model compared to the stellar evolution of Red Giants is that for fuzzballs, a higher temperature and lower radius seems to yield a lower apparent magnitude (m_K). As mention before the luminosity function used in the apparent K-band magnitude calculation for equation (2.7) is written as $L = 4\pi R^2 \sigma_{sb} T^4$. The explanation is that for fuzzballs, the temperature difference between the boundary conditions

are of much larger fraction than that between Red Giants (2500-5000 K). And since $L \propto T^4$ and $L \propto R^2$, this means that temperature play a more vital role for the K-band magnitude. By comparing this to the CDM in figure (3.3) the beginning of the fuzzball models below 9 m_K are more visible than the most luminous and largest Red Giants, making them easier to observe. This however changes quickly because of the short thermal timescale, which can be a good indicator if a fuzzball, or a Red Giant is being observed.

Only until approximately 100 years after the formation of a fuzzball, it is expected to be more difficult to see as the apparent magnitude exceeds 16 magnitudes and it begins to blend in together with the background.

From Mastrobuono-Battisti et al. (2021) the formation rate of WD core fuzzballs are roughly 2100 per Gyr. On the cosmological time scale, this phenomena would be highly unlikely to observe as 100 years is essentially no time at all. If we state that a fuzzball is observable for 100 years with its current formation rate, the fraction of finding one fuzzball per year is $\frac{1200 \cdot 100 \ years}{1 \ Gyr} = 0.00012$. Which is extremely unlikely to observe compared to that of ≈10% of RGs in a population of 60000. The formation rate of NS and BH cores are even smaller, and even with a higher thermal time scale, they are much rarer.

Below in figure (3.8) the change in temperature over time for the different boundary conditions of the WD core fuzzball can be seen. It was achieved by solving equation (2.19) and follows the same boundary conditions for WD core fuzzballs as the previous figure.

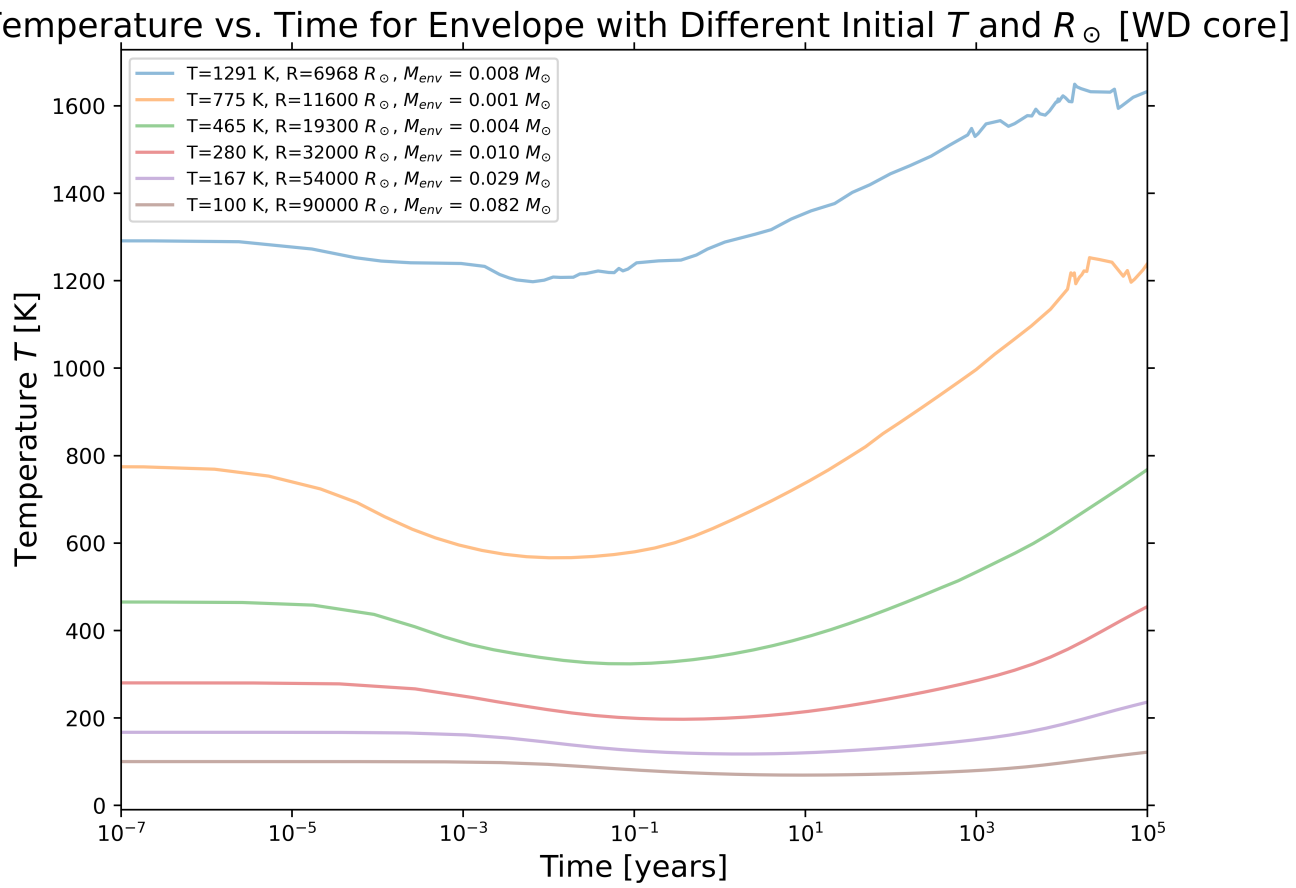

Figure 3.6: How temperature changes with time for the fuzzballs with a WD core for different boundary conditions

In this figure we can follow how the temperature changes together with the K-band magnitude from figure (3.5). It is clear that the same trend for a constant value in the first 8 hours will be present, as the thermal time scale have not yet run its course. From the previous figure the apparent magnitude goes up, while the temperature fluctuates a little bit. After the thermal time scale, the fuzzball has lost its thermal energy. This makes so the envelope starts to contract as nothing is pushing against it. In doing so, the envelope becomes more compact, similarly to how a star behaves, and the pressure increases the temperature. This process will continue until the radius of the envelope has converged to zero. The temperature also increase more for fuzzballs that begins with higher temperatures. As the envelope contracts the temperature first decreases before increasing. The initial decrease comes from the complexity of the opacity for the boundary conditions of the fuzzball. However it then becomes hotter as it contracts.

We can observe the correlation of m_K and temperature with change in radius in figure (3.7) below. It was achieved using equation (2.20) and follows the same boundary conditions as previously for a WD core.

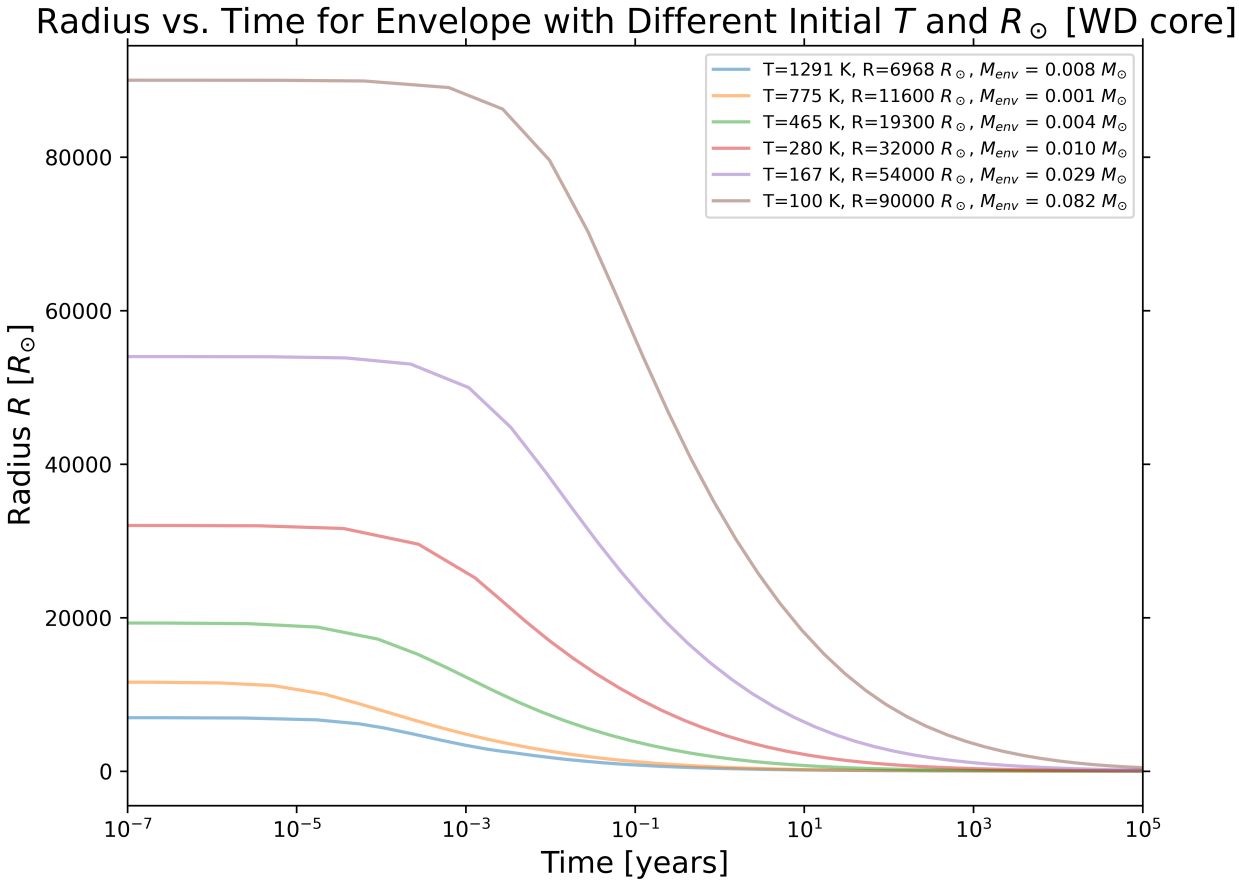

Figure 3.7: How radius changes with time for the fuzzballs vs. as they radiate away

In this figure the change in radius can be observed in correlation to its temperature and m_K for the different boundary conditions. The masses of the envelopes are nowhere near the mass of the core, but the larger the fuzzball, the more mass from the mass transfer has been received. It is noticeable that the radius of the fuzzball decreases after the thermal timescale, as it loses energy at constant envelope mass and seems to converge towards 0. From the previous figure it can be seen that the temperature is increasing as the fuzzballs radius decreases.

The luminosity of these WD core fuzzballs was plotted against its temperature and can be seen in the HR diagram below. To add to the HR diagram, the stellar evolution of a $1M_\odot$ was plotted alongside it. This shows a good illustration of the difference in temperature and luminosity for these two stellar objects.

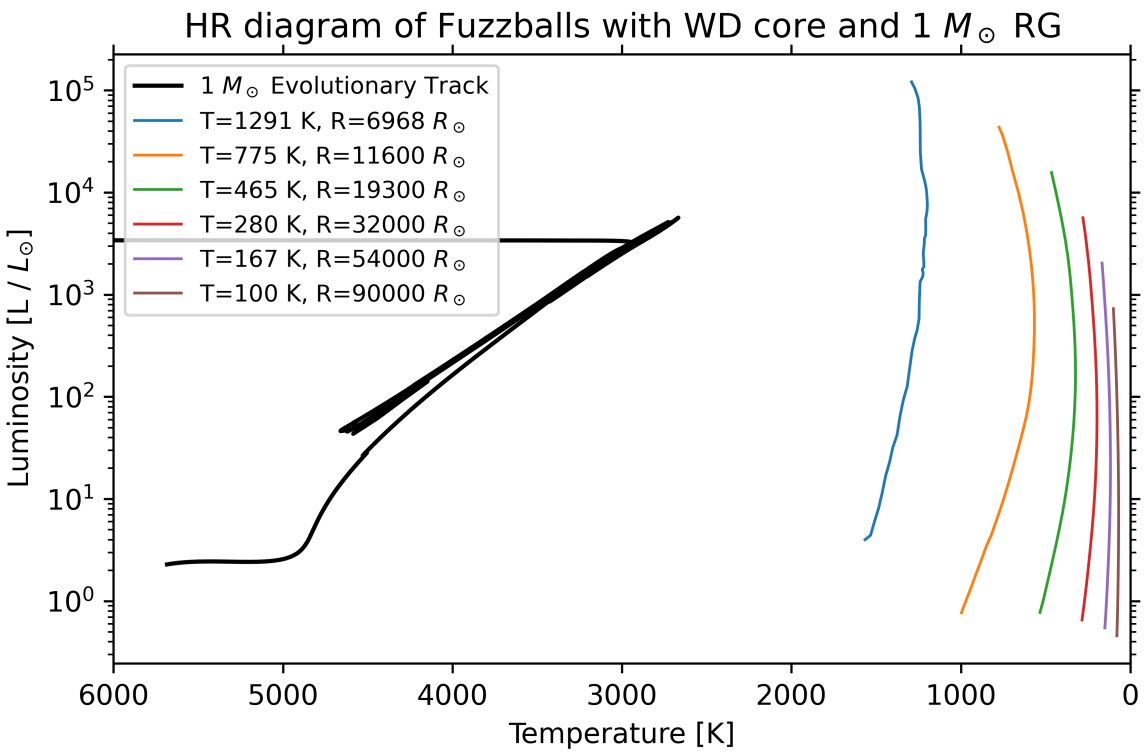

Figure 3.8: This displays a HR digram for a 1 $M_\odot$ RG track together with WD core fuzzballs with the different boundary conditions

This is a good representation of how to tell fuzzballs and Red Giants apart using photometry. The WD core fuzzballs can be much more luminous initially, however they stay around the same cooler temperature compared to the RG stars, which has a higher range and higher temperature. Additionally instead of becoming more luminous as time progresses, they instead decrease in luminosity with a sharp decline in observability, which can be accounted for by the decrease in radius which can be seen in figure (3.7).

Chapter 4

Analysis

The galactic center as mentioned previously contains millions of stars and collisions with only white dwarf cores is therefore unlikely. Red Supergiants have masses well above $10M\odot$ and have been measured in the GC by Hekker (2017). At the end of their life they can either leave a Neutron Star (NS) core or a Black Hole (BH) core. It is possible that those dense compact cores could collide with a still active Red Giant and create fuzzballs with a more massive cores. Below is such a fuzzball model for K-band magnitude where the cores have been exchanged for that of a BH and NS. The same boundary conditions for the WD core are applied from table (2.2).

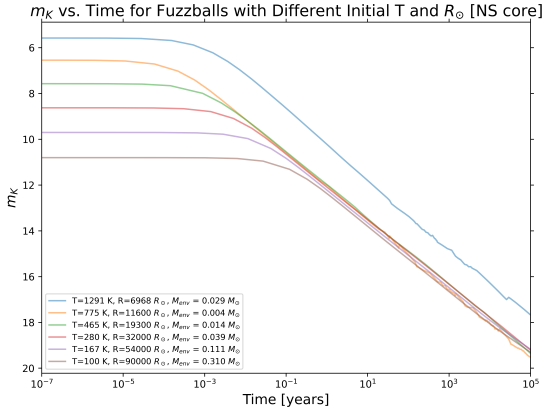

(a) The apparent magnitudes m_K for fuzzballs with NS core [1.4 $M_\odot$] vs. time.

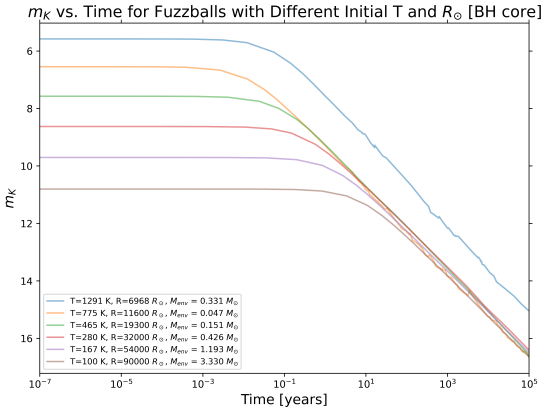

(b) The apparent magnitudes m_K for fuzzballs with BH core [5 $M_\odot$] vs. time.

Figure 4.1: This illustrates how a NS core fuzzballs apparent K-band magnitude changes with time compared to BH core fuzzballs.

An immediate observation can be made when comparing figure WD core fuzzballs (3.5) with this figure, and that is that the thermal timescale is longer the heavier the core mass is. This is unsurprising as the heavier core mass also accumulate a heavier envelope mass because of the larger gravitational pull. This in addition leads to a lower magnitude for

a longer period of time. A fuzzball with a BH core formed 100000 years ago would still be observable today, a NS core would only be observable for 10000 years before beginning to become too faint as m_K goes above 16 magnitudes. To compare this with WD core fuzzballs from figure (3.5), they would be difficult to observe after 10 years after formation, and becoming too faint to observe after 100 years .

From both the WD core fuzzballs and BH/NS core fuzzballs the blue line with boundary conditions $T = 1291\ K$ and $R = 6968 R_\odot$ have a different behavior compared to the others. It can be explain by looking at Mastrobuono-Battisti et al. (2021) paper, where the fuzzballs with those boundary conditions falls into another branch that accumulates a little bit more envelope mass despite its lowest radius. The fluctuations at roughly 50 years for the NS cores and 70 years for the BH cores are where the fuzzball models fails, which will be more clear in figure (4.3) further below.

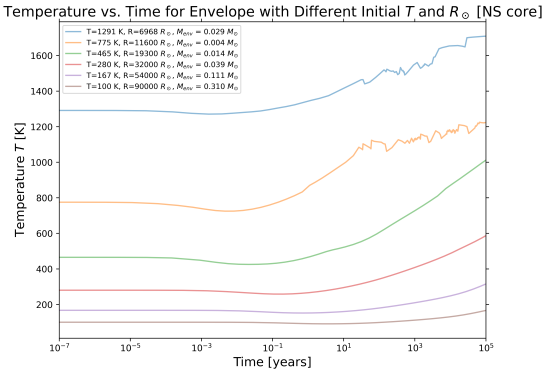

(a) How temperature changes with time for the fuzzballs with a NS core [1.4 $M_\odot$]

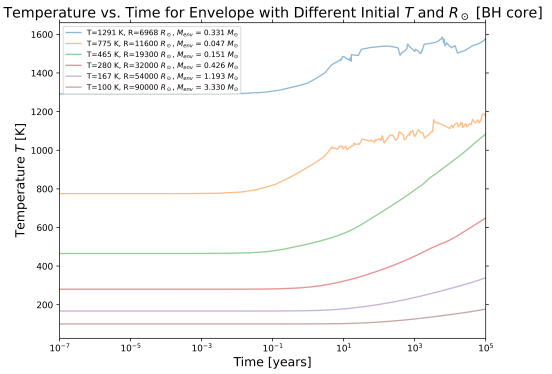

(b) How temperature changes with time for the fuzzballs with a BH core [5 $M_\odot$]

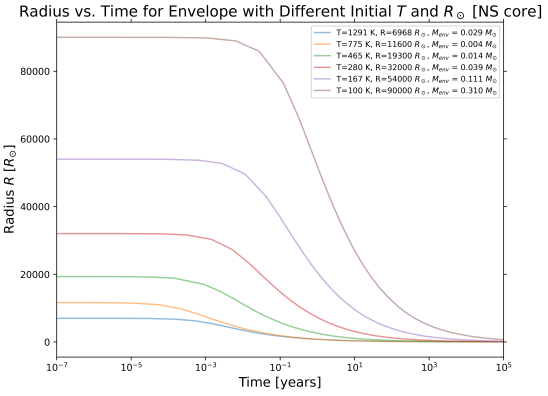

(c) How radius changes with time for the fuzzballs with a NS core [1.4 $M_\odot$]

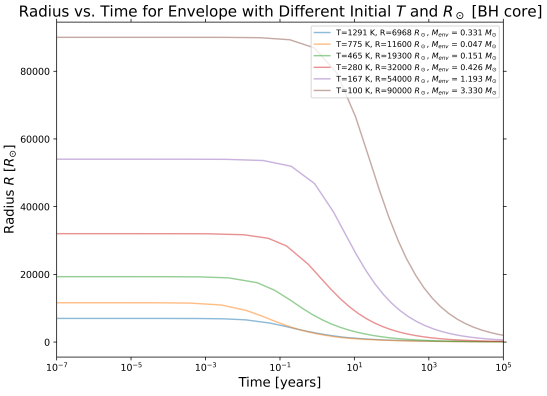

(d) How radius changes with time for the fuzzballs with a BH core [5 $M_\odot$]

Figure 4.2: This illustrates how NS core fuzzballs radius and temperature changes with time compared to BH core fuzzballs.

In figure (4.2) the relation between the different core masses for their temperature and

radius can be seen, and it similarly follows the same trend as the WD core. The main difference again being that the longer thermal timescale makes the heavier core's envelope contract at a later stage, hence making its temperature increase at the same later stage. The fluctuations for BH cores at 70 years in figure (4.4a), and for NS core at 50 years in figure (4.4b) are much more noticeable here. In figure (4.4a) and (4.4b) The model evidently fails for both NS cores and BH cores for the boundary conditions of $T = 1291$ K, $R = 6869\ R_\odot$ and $T = 775$ K, $R = 11600\ R_\odot$, as can be seen by the fluctuations. .

The fuzzball model breaks down after attempting to solve equation (2.16) for constant mass envelope and equation (2.17) says that the change in energy is equal to -L, which means that radius must decrease. The fuzzball then follows the line of the two equation solutions, but then reaches a turning point which can be seen in Mastrobuono-Battisti et al. (2021). At that point, the two equations can not simultaneously be satisfied. This means that the fuzzballs cease to behave and does not have any solutions, thus creating the fluctuation. It can be seen in the figure below that the fuzzball misbehaves and constant mass of the envelope is broken.

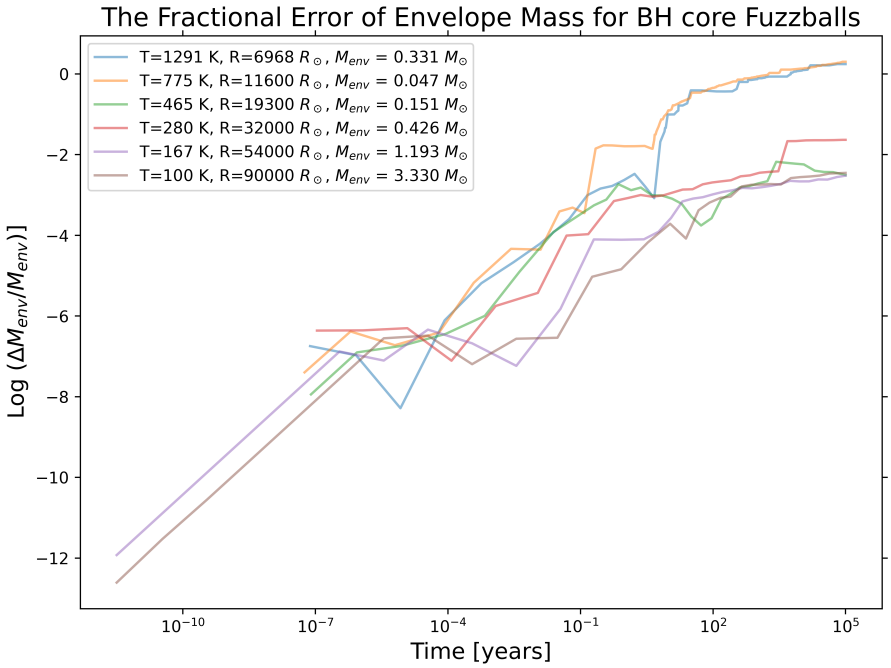

Figure 4.3: This shows the fractional error of the envelope mass in a fuzzball with a BH core with the set of initial boundary conditions.

In the figure the solution accuracy The -2 line corresponds to 1% meaning that the fractional errors are really good below that line and the envelope mass behaves, as seen in previous figures. The blue and orange line goes above the -2 line and hence creates a larger fractional error for the envelope mass and shows that the mass conservation cannot be satisfied when the fuzzballs attempts to evolve.

The fuzzball model can additionally be utilized to check if G2 is a fuzzball. G2 refers to a gas cloud in orbit around the SMBH, and the origin for this cloud is still being debated. In 2014, when G2 was at its closest distance to the SMBH, it did not get disrupted as expected; instead, it maintained its structure. This suggests that the cloud might be self-gravitating. One possible explanation for this, and why fuzzballs are so interesting, could be the presence of a dense core within the gas cloud, which would make it a fuzzball. Plewa et al. (2017). Observations of the G2 gas cloud have measured its temperature to be $T = 560$ K and $R = 570\ R_\odot$ from Witzel et al. (2014). By calculating the thermal time-scale from equation (2.15), it can be concluded that a WD core is too small, as the thermal time-scale is too short (see figure (4.4a) below). This result was also established in the Mastrobuono-Battisti et al. (2021) paper. The formation rate of NS core are very small and although it has a longer observable time, it is still unlikely. This infers that if the G2 cloud is a fuzzball, the core must be of larger mass than a WD. A BH core seems to be a viable fit for the G2 model because of its long thermal time-scale and observability, however it was said in Mastrobuono-Battisti et al. (2021) that the formation rates of such cores are the lowest and therefore not convincing. If G2 however is a fuzzball, it must then be over 100 000 years, as its reported K-band magnitude is $m_K = 18$ from Gillessen et al. (2012b). Which would mean its thermal timescale has surpassed for BH cores and the magnitude should continue to decrease as time progresses.

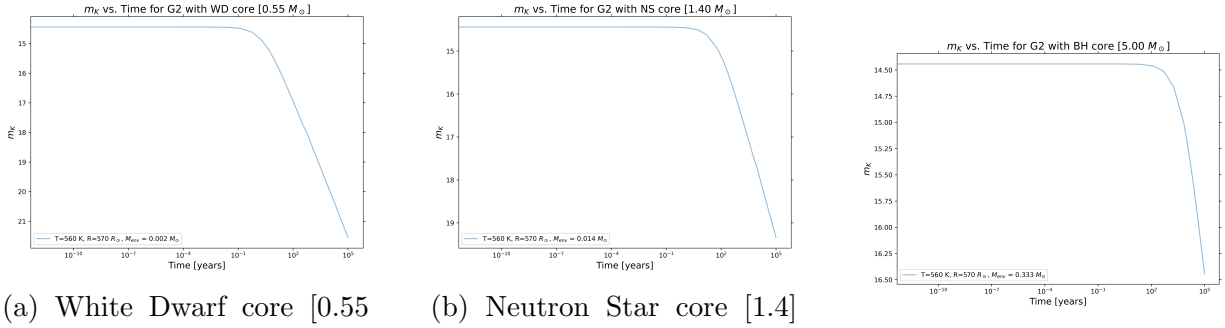

(a) White Dwarf core [0.55 $M_\odot$]

(b) Neutron Star core [1.4] $M_\odot$

(c) Black Hole core [5 $M_\odot$]

Figure 4.4: This shows at what magnitude the G2 cloud as a fuzzball and how it changes depending on which core type

Table 4.1: Different cores for the G2 cloud observed in the galactic center with $T = 560$ K and $R = 570\ R_\odot$

Core Type	$\tau_{th,env}$ [Years]
White Dwarf (WD)	4.314
Neutron Star (NS)	110.130
Black Hole (BH)	9299.030

The question then remains of how do we know if we are observing a fuzzball or a RG star after during/after its Red Clump stage? Because of the initial mass function there is a majority of lower-mass stars present in the GC, hence WD-cores would then be in the majority after the star has run its course. By continuous observations it should then be concluded that fuzzballs with such a core radiate away and loose their visibility entirely after a 100 years due to the sharp decrease in luminosity. In the cosmological time frame, formations of massive cored fuzzballs are even less likely than WD cores, as shown by Mastrobuono-Battisti et al. (2021), and should definitely not be the first guess when observing objects in the GC.

As shown in figure (2.1) and figures (3.2) RGs star have much higher temperatures compared to the observable fuzzballs. Spectroscopy could then show absorption lines that are typical for forming Red Giants which would not be present in fuzzballs of those temperatures. Additionally if it is a new formed fuzzball, it will have a significantly higher luminosity, but will decrease over time, while a observable RG after the RC phase will increase in luminosity. The decrease in luminosity is related to the increase in K-band magnitude, hence making it fainter as the envelope shrinks.

4.1 Conclusion

In this thesis stellar evolution tracks from MIST was utilized in a semi-analytical model python code to get the the apparent magnitude in the K-band (near infra-red). With this, a 1000 star simulation was created for stars between the ages of 10-12 Gyrs where a initial mass range of $0.96 - 1.02\ M_{\odot}$ was established to have their Red Giant phase within that time condition. By running the simulation through the initial mass function it showed that the closer the Red Giants are to dying, the redder and brighter it so, with a minimum value of approximately $m_K = 10$. Reiterating the process for 60 000 Red Giants to create a stellar population, the result showed that the Red Clump branch of the stars was just around the dropout value for observable magnitudes in GC observations at ($m_K \geq 16$). The conclusion can be drawn that stars during and after the Red Clump branch are differentiable from late stars and observable using photometry and spectroscopy. However such stars become rarer and rarer the lower the magnitude, because of the much shorter expected lifetime at those phases. Only roughly 12% of a population of RGs are observable during and after the RC. This entire process does however not take into account the formation of giant stars, like red supergiants, which have a much lower K-band magnitude, however they are much rarer in their formation rate since the majority of star formation in the GC took place 10 Gyrs ago according to Schödel et al. (2020) and the formation follows the initial mass function.

The Red Giants after their lifetime leaves a dense core that have the possibility to receive an envelope from a mass transfer during a collision. In doing so it was established that mass transfer that happened at a boundary where the mass is just bound, are similarly visible for observations. The time take for the envelope to begin contracting, increasing its

temperature, depends on the thermal time scale, which depends on the mass of the core. It was established that WD cores with 0.55 $M\odot$ have $\tau_{th,env} = 4.3$ Years which means they will not be observable after 100 years. The low fraction of 0.00012 for having an observable WD core fuzzball per year tells us that they are highly uncommon. NS- and BH cores have a longer thermal time scale and hence can be difficult to separate from a RG by observing the apparent K-band magnitude. However because of the temperature difference of the fuzzball compared to the RG, and that fuzzballs become less luminous as time progresses, photometry should be able to tell the difference with observations years apart. From this it can also be said that the G2 cloud orbiting the SMBH cannot be a fuzzball with a WD core. It more points towards a BH core, however they are as mentioned extremely rare. If it is a fuzzball with a BH core, it must be very old, since the observations show that G2 have a K-band magnitude of roughly 18, meaning that the fuzzball must have passed the thermal time scale.

Acknowledgements

I would very much like to thank the kind and engaging people at the Astrophysics Division at Lunds University for making me feel welcome and showing support during this project. I would also like to thank my family and friends for making sure it was going forward and being curious in what I was doing. Lastly and most importantly I want to thank my supervisor Ross Church for introducing me to the field of research. It has been a pleasure learning and diving into the field of research as an astrophysicist and I am very appreciative of this experience.

Bibliography

Abuter, R., Amorim, A., Bauböck, M., Berger, J. P., Bonnet, H., Brandner, W., Clé net, Y., du Foresto, V. C., de Zeeuw, P. T., Dexter, J., Duvert, G., Eckart, A., Eisenhauer, F., Schreiber, N. M. F., Garcia, P., Gao, F., Gendron, E., Genzel, R., Gerhard, O., Gillessen, S., Habibi, M., Haubois, X., Henning, T., Hippler, S., Horrobin, M., Jiménez-Rosales, A., Jocou, L., Kervella, P., Lacour, S., Lapeyrère, V., Bouquin, J.-B. L., Léna, P., Ott, T., Paumard, T., Perraut, K., Perrin, G., Pfuhl, O., Rabien, S., Coira, G. R., Rousset, G., Scheithauer, S., Sternberg, A., Straub, O., Straubmeier, C., Sturm, E., Tacconi, L. J., Vincent, F., von Fellenberg, S., Waisberg, I., Widmann, F., Wieprecht, E., Wiezorrek, E., Woillez, J., and Yazici, S.: 2019, *Astronomy &amp Astrophysics* **625**, L10

Allen, C. W.: 1973, *Astrophysical quantities*

Bartko, H., Martins, F., Trippe, S., Fritz, T. K., Genzel, R., Ott, T., Eisenhauer, F., Gillessen, S., Paumard, T., Alexander, T., Dodds-Eden, K., Gerhard, O., Levin, Y., Mascetti, L., Nayakshin, S., Perets, H. B., Perrin, G., Pfuhl, O., Reid, M. J., Rouan, D., Zilka, M., and Sternberg, A.: 2009, *The Astrophysical Journal* **708(1)**, 834–840

Bosma, A.: 2023, *Rotation curves and the dark matter problem*

Bower, G. C., Markoff, S., Dexter, J., Gurwell, M. A., Moran, J. M., Brunthaler, A., Falcke, H., Fragile, P. C., Maitra, D., Marrone, D., Peck, A., Rushton, A., and Wright, M. C. H.: 2015, *The Astrophysical Journal* **802(1)**, 69

Calderón, D., Cuadra, J., Schartmann, M., Burkert, A., Plewa, P., Eisenhauer, F., and Habibi, M.: 2018, *Monthly Notices of the Royal Astronomical Society* **478(3)**, 3494

Choi, J., Dotter, A., Conroy, C., Cantiello, M., Paxton, B., and Johnson, B. D.: 2016, *The Astrophysical Journal* **823(2)**, 102

Eker, Z., Bakış, V., Soydugan, F., and Bilir, S.: 2021, *Monthly Notices of the Royal Astronomical Society* **503(3)**, 4231

Ferguson, J. W., Alexander, D. R., Allard, F., Barman, T., Bodnarik, J. G., Hauschildt, P. H., Heffner-Wong, A., and Tamanai, A.: 2005, *The Astrophysical Journal* **623(1)**, 585

Figer, D. F., Rich, R. M., Kim, S. S., Morris, M., and Serabyn, E.: 2004, *The Astrophysical Journal* **601(1)**, 319

Gao, J., Li, A., and Jiang, B. W.: 2013, *Earth, Planets and Space* **65(10)**, 1127

Gillessen, S., Genzel, R., Fritz, T. K., Quataert, E., Alig, C., Burkert, A., Cuadra, J., Eisenhauer, F., Pfuhl, O., Dodds-Eden, K., Gammie, C. F., and Ott, T.: 2012a, *Nature* **481(7379)**, 51

Gillessen, S., Genzel, R., Fritz, T. K., Quataert, E., Alig, C., Burkert, A., Cuadra, J., Eisenhauer, F., Pfuhl, O., Dodds-Eden, K., Gammie, C. F., and Ott, T.: 2012b, *Nature* **481(7379)**, 51

Hannu Karttunen, Pekka Kröger, H. O. M. P. K. J. D.: 2016, *Fundamental Astronomy*, Springer Berlin Heidelberg, Berlin

He, X.-J., Luo, A.-L., and Chen, Y.-Q.: 2022, *Monthly Notices of the Royal Astronomical Society* **512(2)**, 1710–1721

Hekker, S.: 2017, *Asteroseismology of Red Giants and Galactic Archaeology*, p. 95–117, Springer International Publishing

Kong, Q., Siauw, T., and Bayen, A. M.: 2021, in Q. Kong, T. Siauw, and A. M. Bayen (eds.), *Python Programming and Numerical Methods*, pp 295–313, Academic Press

Kroupa, P. and Weidner, C.: 2003, *ApJ* **598(2)**, 1076

Laurentis, M. D., de Martino, I., and Monica, R. D.: 2023, *Reports on Progress in Physics* **86(10)**, 104901

Lejeune, T., Cuisinier, F., and Buser, R.: 1998, *Astronomy and Astrophysics Supplement Series* **130(1)**, 65

Mastrobuono-Battisti, A., Church, R. P., and Davies, M. B.: 2021, *Monthly Notices of the Royal Astronomical Society* **505(3)**, 3314

NASA, *Infrared: Beyond the Visible*, Accessed on November 27th, 2023

Neumayer, N., Seth, A., and Böker, T.: 2020, *The Astronomy and Astrophysics Review* 28(1)

Nogueras-Lara, F., Schödel, R., and Neumayer, N.: 2021, *Astronomy &amp Astrophysics* **653**, A133

Phifer, K., Do, T., Meyer, L., Ghez, A. M., Witzel, G., Yelda, S., Boehle, A., Lu, J. R., Morris, M. R., Becklin, E. E., and Matthews, K.: 2013, *The Astrophysical Journal Letters* **773(1)**, L13

Plewa, P. M., Gillessen, S., Pfuhl, O., Eisenhauer, F., Genzel, R., Burkert, A., Dexter, J., Habibi, M., George, E., Ott, T., Waisberg, I., and von Fellenberg, S.: 2017, *The Astrophysical Journal* **840(1)**, 50

Prialnik, D.: 2000, *An Introduction to the Theory of Stellar Structure and Evolution*, Cambridge University Press, Cambridge

Rafelski, M., Ghez, A. M., Hornstein, S. D., Lu, J. R., and Morris, M.: 2007, *ApJ* **659(2)**, 1241

Schödel, R., Nogueras-Lara, F., Gallego-Cano, E., Shahzamanian, B., Gallego-Calvente, A. T., and Gardini, A.: 2020, *Astronomy &amp Astrophysics* **641**, A102

Schödel, R., Najarro, F., Muzic, K., and Eckart, A.: 2010, *AA* **511**, A18

Thompson, T.: 2014, *Astronomy 1101 — Planets to Cosmos*, Accessed on November 27th, 2023

Witzel, G., Ghez, A. M., Morris, M. R., Sitarski, B. N., Boehle, A., Naoz, S., Campbell, R., Becklin, E. E., Canalizo, G., Chappell, S., Do, T., Lu, J. R., Matthews, K., Meyer, L., Stockton, A., Wizinowich, P., and Yelda, S.: 2014, *The Astrophysical Journal* **796(1)**, L8

Wollack, D. E. J.: Friday, 04-16-2010, *The Life and Death of Stars*, Accessed on November 24th, 2023

Xiang, M. and Rix, H.-W.: 2022, *Nature* **603(7902)**, 599–603

Zheng, L. and Zhang, X.: 2017, in L. Zheng and X. Zhang (eds.), *Modeling and Analysis of Modern Fluid Problems*, Mathematics in Science and Engineering, pp 361–455, Academic Press